CrossMark

Effect of Fe doping on the photocatalytic activity of ZnO nanoparticles: experimental and theoretical investigations

B. Radha[1] · R. Rathi[2] · K. C. Lalithambika[1] · A. Thayumanavan[1] · K. Ravichandran[3] · S. Sriram[1]

Abstract

Pure and Fe doped ZnO nanoparticles were prepared by a facile and cost-effective co-precipitation method. The X-ray diffractograms (XRD) reveal that the grown nanoparticles are hexagonal in structure and the crystallite sizes are in the range of 27–28 nm. The transmission electron microscope (TEM) micrographs confirmed the spherical nature of the grown particles and the Fourier transform-infrared (FT-IR) studies confirmed the presence of Zn–O bonding in the prepared nanoparticles. Additionally, the presence of the constituent elements is confirmed with XPS analysis. The optical bandgap of the prepared nanoparticles are calculated as 3.28, 3.19 and 3.08 eV for ZnO, ZnO–Fe 10 at.% and ZnO–Fe 20 at.%, respectively. The photocatalytic dye degradation efficiency against methylene blue, is 68.52, 73.96, and 87.92, respectively. To validate the photocatalytic activity, a DFT based calculation was performed to measure the band edge positions of the pure and Fe doped ZnO nanostructures, and the obtained results are well supported by the experimental results.

1 Introduction

The environment is polluted continuously due to the growth of industries and their untreated effluents. Organic dyes are one of the most polluting factors from textile industries because they are non-biodegradable and toxic. To avoid the contamination effect caused by organic dyes, there is a need for proper effluent cleaning system adopted in the textile industries. Generally, textile industry effluents contain a large number of organic dyes which are harmful to living species as well as the lands nearby the industries. During the dyeing process, a large number of effluents are released with high toxicity which infertile the surrounding areas. To avoid this situation, many types of research are going on to find an efficient methodology regarding cost wise and power consumption wise. Among the methods, the photocatalytic process is one, in which semiconductors are used to degrade many organic dyes [1]. Photocatalysts based on ZnO have been identified as an efficient candidate to remove organic pollutants in water through UV light irradiation. ZnO is a very attractive semiconductor photocatalyst for its wide bandgap of 3.366 eV [2], and it has large exciton binding energy of 60 meV at room temperature [3]. However, ZnO based semiconductors are limited because of their higher charge carrier recombination rate. To avoid the recombination of photogenerated electron and hole pairs in ZnO based nanosized materials, transition metals have been widely employed as dopants due to their lower cost and abundance. ZnO nanoparticles with various dopants are reported in the literature [4–10]. Among them, Fe is one of the most suitable candidate for ZnO lattice because of its highly interacting 3d orbitals. Fe doped ZnO nanoparticles are prepared by various methods [11–15], and only very few reports are based on co-precipitation method [16]. The advantage of co-precipitation method is the precursor is formed by atomic scale mixing which requires the calcination process and leads to the formation of particles of lesser size. Here in this present work, it is aimed to prepare a facile and cost-effective fabrication of Fe doped ZnO nanoparticle as an efficient photocatalyst for organic dye degradation. Also, a theoretical calculation is performed using DFT to get insight about the electronic band edges of the prepared samples.

✉ S. Sriram
   sukansriram@gmail.com

[1] Department of Physics, School of Electrical & Electronics Engineering, SASTRA Deemed University, Thanjavur, Tamil Nadu 613401, India

[2] Department of Physics, Sengamala Thayaar Educational Trust Women's College, Mannargudi 614016, Tamil Nadu, India

[3] P.G and Research Department of Physics, AVVM Sri Pushpam College, Poondi, Thanjavur 613501, Tamil Nadu, India

2 Experimental details

Pure and Fe doped ZnO nanoparticles were prepared by a simple and cost-effective soft chemical method (co-precipitation method) [17]. For the preparation of ZnO nanoparticles, 0.1 M of Zinc Acetate dihydrate was dissolved in 100 mL of deionized water with continuous stirring. After the homogeneous precursor formation, NaOH was added drop-by-drop inorder to maintain the pH value of the solution at 8. This mixture was heated at 85 °C for 2 h with continuous stirring with a magnetic stirrer. Then the solution was allowed to cool at room temperature and kept for 24 h without any disturbances. A white precipitate was obtained, and it was filtered and washed using a mixture of water and ethanol in the ratio of 3:1. The obtained products were dried then at 110 °C for 30 min.

Fe doped ZnO nanoparticles were prepared using Ferric chloride as a precursor for Fe with the same preparative procedure and condition. Finally, all the prepared samples were annealed at 400 °C for 2 h in normal atmosphere and allowed to cool until it reaches room temperature.

2.1 Characterization

The structural characteristics of the prepared ZnO and Fe doped ZnO nanoparticles have been studied by X-ray powder diffraction technique (PAN-analytical-PW 340/60 X'pert Pro) with 2θ step size of 0.05. The microstructure analysis is performed using field emission–transmission electron microscope (FE–TEM) and the Fourier transform infrared spectra (FTIR) were recorded using FTIR spectrometer in the range 4000–400 cm^{-1} (Spectrum 100, Perkin Elmer, USA). X-ray photoelectron spectroscopy (XPS) was performed on an (ESCALAB 250, Thermo Scientific) X-ray photoelectron spectrometer with binding energy calibration of C 1s (C–C—285 eV). Optical properties of the prepared nanoparticles were measured using UV–Vis-NIR spectrophotometer with wavelength step size of 1 nm.

2.2 Evaluation of methylene blue degradation

The photocatalytic activities of the prepared nanoparticles were evaluated against the methylene blue (MB) dye in aqueous media under visible light radiation using Xe arc lamp (300 W). 50 mg of the prepared nanoparticles were dissolved in 100 mL MB aqueous solution (1×10^5 M) separately and stirred in the dark atmosphere until adsorption–desorption equilibrium is reached. Under the ambient atmospheric condition, the mixture was exposed to Visible light. On every 15 min of interval, the reaction solutions were centrifuged and filtered to remove the residues. The photocatalytic reaction

was monitored by recording the absorption spectrum of the MB (λ = 664 nm) dye in the reaction solution for every 15 min using a UV–Vis spectrophotometer (Systronics 2003).

2.3 Computational method

For theoretical validation, first principle calculations were carried out using density functional theory (DFT) implemented in SIESTA [18] package. Supercells of ZnO, Fe doped ZnO, were constructed and optimized to ground state energy using conjugate gradient method. For the exchange–correlation energy calculation, generalized gradient approximation (GGA) with PBE functional [19], and norm-conserving potential for *core*-valence interaction was employed. The double zeta plus (DZP) polarization orbitals were used for the valence electrons. In this calculation, 3d, 4s states of Fe and Zn atoms, and 2s and 2p states of O atom were considered. For the electronic structure calculations, the Brillouin zone integration was done using a $5 \times 5 \times 5$ k-points sampling grid. The energy cut-off of 300 eV was used for all the calculations, and the structures were fully relaxed until the forces were less than 0.05 Å. For convenience, the structures were named as ZnO, Fe_{10}@ZnO, and Fe_{20}@ZnO. The optimized structures were shown in Fig. 1.

3 Results and discussion

3.1 Structural studies

The XRD patterns of ZnO and Fe doped ZnO (10, 20 at.%) nanoparticles are depicted in Fig. 2. For ZnO nanoparticles (Fig. 2a), the observed peaks are related to (100), (002), (101), (102), (110), (103), (200), (112) and (201) lattice planes. These peaks correspond to hexagonal wurtzite of ZnO (JCPDS card no 65-3411). The preferential orientation for the prepared ZnO nanoparticles is observed along the (101) plane. For the Fe doped ZnO nanoparticles, apart from the ZnO designated peaks, a small peak around 27° was observed. This may be due to the incorporation of Fe ions into the ZnO lattice. This peak is matched with FeO phase of iron oxide hydroxide (JCPDS card no 89-6096). When the Fe concentration is increased, the peak intensity increased. This confirms that the extra peaks are due to the incorporation of Fe dopant. However, the preferential growth is not changed even Fe is added to the ZnO lattice.

The crystalline size of the prepared ZnO and Fe doped ZnO nanoparticles were calculated using Scherrer's formula [20]

$$D = \frac{0.9\lambda}{\beta \cos \theta} \qquad (1)$$

where, λ is Cu-Kα radiation (1.5406 Å), 0.9 is the shape factor value, θ is the Bragg's angle, and β is the full width at half maximum (FWHM). The lattice constants for the

Fig. 1 Structures of ZnO and Fe doped ZnO supercells

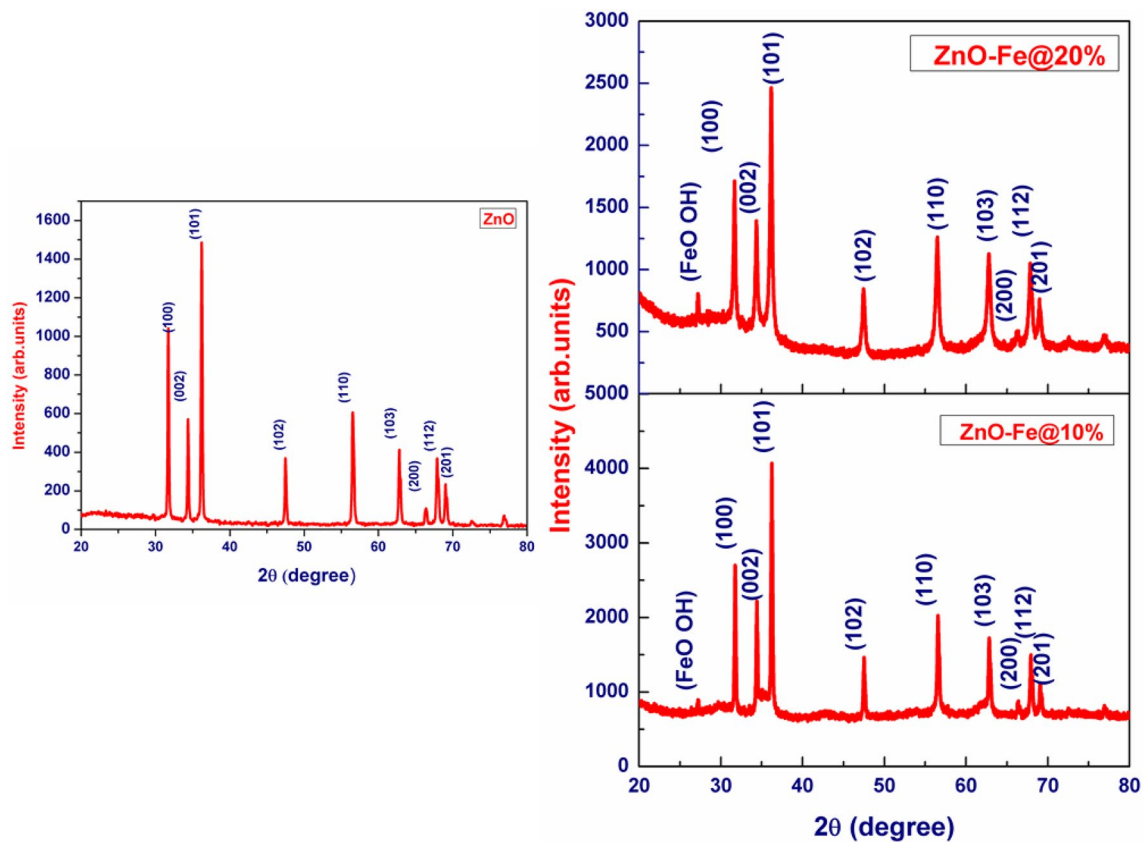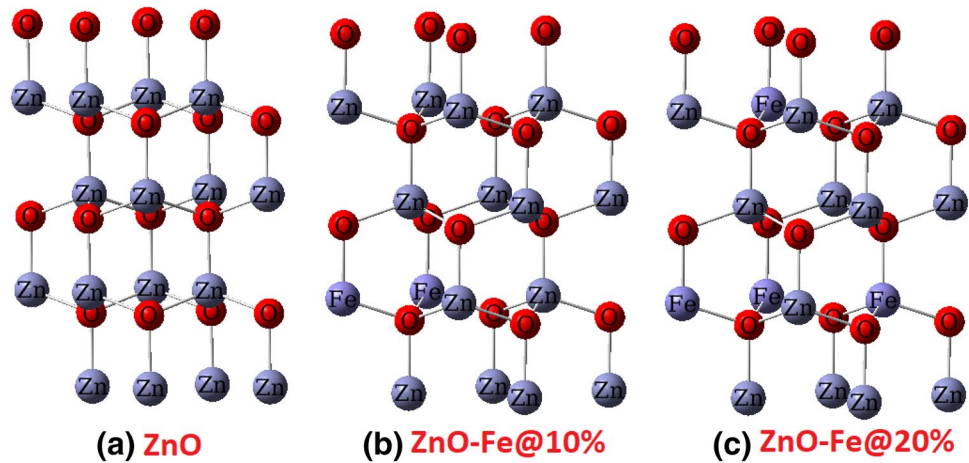**(a) ZnO**　　　　**(b) ZnO-Fe@10%**　　　　**(c) ZnO-Fe@20%**

Fig. 2 XRD patterns of **a** ZnO, **b** Fe 10 at.% doped ZnO and **c** Fe 20 at.% doped ZnO

hexagonal structures (a & c) are calculated using the following formula [21]

$$\frac{1}{d^2} = \frac{4}{3} + \frac{(h^2 + k^2 + hk)}{a^2} + \frac{l^2}{c^2} \qquad (2)$$

where d is the interplanar distance and hkl are Miller indices.

The volume of the crystallites was calculated using the following formula [22]

$$V = \frac{\sqrt{3}}{2} a^2 c \qquad (3)$$

The calculated structure parameters are listed in Table 1. It can be seen that the calculated crystallite sizes of all the nanoparticles are almost consistent with each other and reveals the controlled growth of the ZnO nanoparticles. From the calculated lattice constant values, it is seen that Fe doped ZnO nanoparticles have lesser value compared to pure ZnO nanoparticles. This may be due to the substitutional effect of Fe^{3+} ion which has a lesser ionic radius (0.645 Å) than the Zn^{2+} ionic (ionic radius = 0.74 Å) site in the ZnO lattice. The calculated unit cell volume is consistent with the prepared nanoparticles and has the same hexagonal wurtzite lattice.

3.2 Microstructural analysis

The transmission electron micrograph of Fe doped ZnO nanoparticles is shown in Fig. 3. From the figure, it can be seen that the prepared particles are spherical with an average crystallites size of 25 nm. This result is in good agreement

Table 1 Crystallite size, lattice parameters and unit cell volume of the prepared nanoparticles

Sample	Crystallite size (D) nm	Lattice constant		Unit cell volume ($Å^3$)
		a (Å)	c (Å)	
ZnO	28.26	3.2519	5.21506	47.75860
ZnO–Fe 10 at.%	27.84	3.2499	5.20594	47.61645
ZnO–Fe 20 at.%	28.88	3.2540	5.21356	47.80655

Standard values a = 3.249 Å and c = 5.206 Å—JCPDS card no 65-3411

with crystallite sizes calculated with XRD data. It is also noted that the grains are evenly distributed, and this may be attributed to the small size of the nanoparticles with high surface energy.

3.3 FTIR spectrum analysis

The vibrational bands and the functional groups present in the prepared nanoparticles were analyzed by taking FT-IR spectrum at room temperature. The FT-IR spectra of undoped and Fe doped ZnO are shown in Fig. 4. Solid phase FT-IR spectra were recorded between 4000 and 400 cm^{-1}. In FT-IR spectrum, the presence of inorganic elements is associated with the band frequencies around 1000 cm^{-1}. The undoped ZnO and Fe doped ZnO FTIR spectra interpretations are explained in Table 2. This confirms the presence of ZnO–Fe local bands and defect states besides the formation of wurtzite structure [23, 24]. This peak is also attributed to the bond between iron and oxygen (Fe–O). The observed results of the FT-IR spectra, for the Fe doped ZnO, is consistent with the XRD profile and confirms the formation of ZnO–Fe.

3.4 XPS analysis

The surface composition and chemical valance states of the individual elements present in the prepared Fe–ZnO nanoparticles are shown in Fig. 5a. From the spectrum, it is seen that a strong peak is observed at 1021.4 eV corresponds to Zn 2p state. High-resolution spectra of the constituent elements are shown in Fig. 5b. From the figure, it can be seen
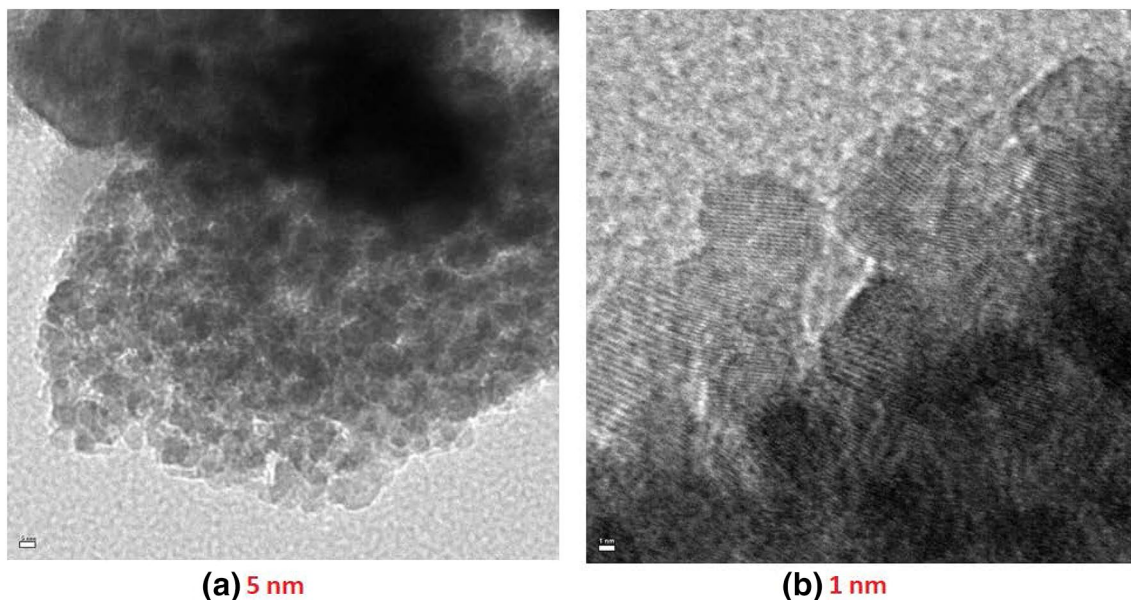

(a) 5 nm

(b) 1 nm

Fig. 3 TEM micrographs of ZnO–Fe@20% nanoparticles
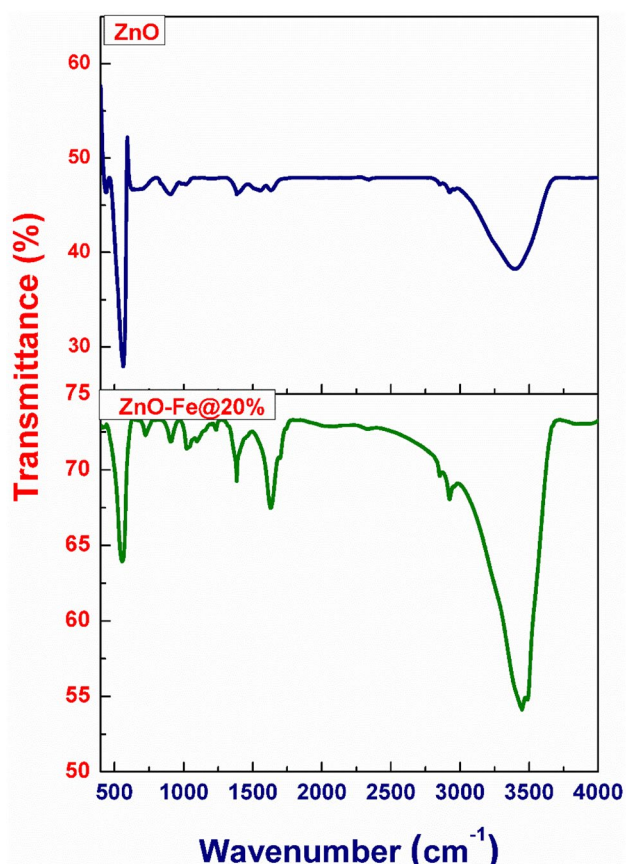
Fig. 4 FTIR spectra of ZnO and ZnO–Fe@20% nanoparticles

that O 1s region is confirmed with the peak at 530.5 eV and this can be attributed as O^{2-} ion deficient region. The peak observed at 710.9 eV is attributed as Fe 2p state [25]. From the results, it is evident that the Fe^{3+} ions are present in the ZnO lattice.

3.5 Optical properties

The optical absorbance spectrum of ZnO and Fe doped ZnO nanoparticles are shown in Fig. 6. From the figure, it can be seen that the absorption edge moves towards the higher wavelength region with the increase of Fe doping percentage. The reason may be ascribed as upon Fe doping more active sites are formed which leads to more absorption of photons incident on it. This results in the increase of photocatalytic performance of the Fe doped ZnO nanoparticles compared to undoped ZnO nanoparticles. The band gap of the nanoparticles can be calculated using the absorption edge wavelength, and the values are 3.28, 3.19 and 3.08 eV for ZnO, ZnO–Fe 10 at.% and ZnO–Fe 20 at.%, respectively. The shifting of bandgap towards lower energy region enhances the transfer of electrons from the valence band to the conduction band, and in turn, increases the photocatalytic efficiency.

3.6 Photoluminescence studies

To examine the crystal quality and purity, photoluminescence studies for the prepared undoped and Fe doped ZnO nanoparticles were carried out. The PL spectra of undoped and Fe doped ZnO are shown in Fig. 7. The spectra of all the nanoparticles exhibit a strong peak at 385 nm attributed to the near band edge (NBE) [26] due to the band to band transition. Another strong shoulder peak observed around 420 nm is due to the recombination of an electron–hole pair in Zn vacancy [27]. From the PL spectra, it is seen that the intensity of the peaks decreases due to doping. It decreases further when the doping concentration is increased. This may be ascribed as the doping of Fe on ZnO lattice that reduces the defects in the Fe–ZnO complex which eventually increases the localized energy levels near the valence band. This reduction in the band gap further increases the photocatalytic efficiency of the nanoparticles. This is well supported by the XRD spectra observed for the prepared nanoparticles.

3.7 Photocatalytic studies

The photocatalytic activity of ZnO and Fe doped ZnO nanoparticles were evaluated for MB dye degradation under visible light illumination. Since MB has a characteristic peak of absorption at 663 nm; it was used as a reference for the

Table 2 Interpretations of FTIR spectra of ZnO and 20% Fe doped ZnO nanoparticles

ZnO spectra bands (cm^{-1})	Fe doped ZnO spectra bands (cm^{-1})	Peaks interpretation
3388	3422	Stretching mode (ν)of a hydroxyl group(O–H) or the water molecules present in the surface
~2900	2922	Stretching vibration (ν) of CH_2-and-CH_3-groups
~1650	1626	ν_{asy} C=O
~1590	1568	ν_{sy} C=O
–	1384	Vibration of Zn–O–Fe local band
569	567	ν Zn–O. Also ν Fe–O for Fe doped ZnO

Fig. 5 **a** XPS spectra of Fe doped ZnO nanoparticles **b** high resolution spectra of Zn 2p, Fe 2p and O1s regions
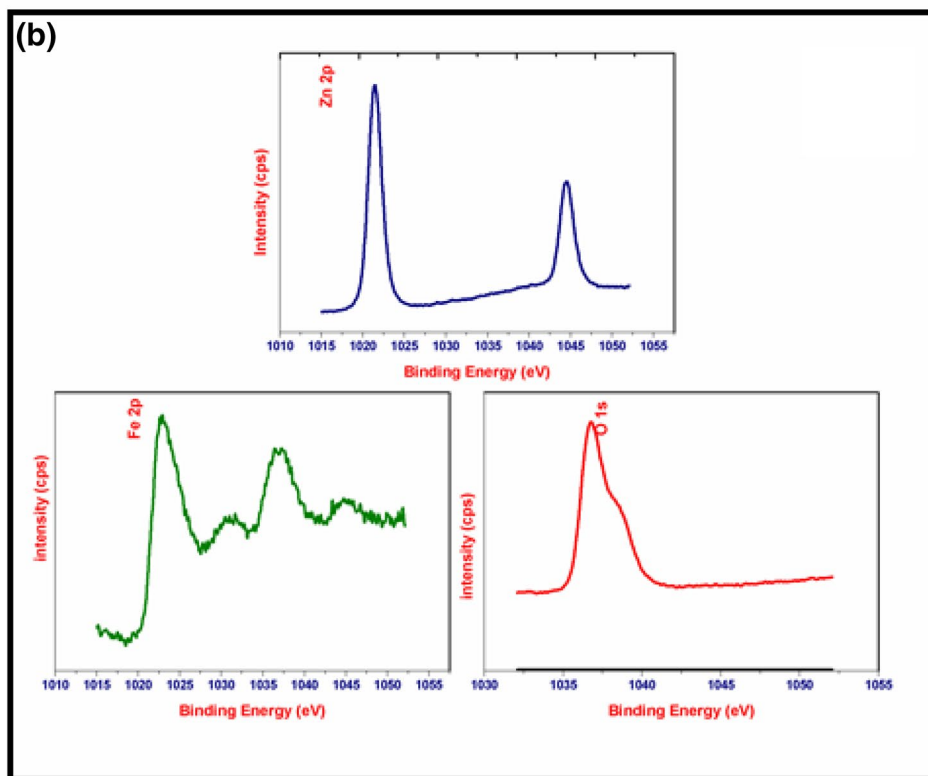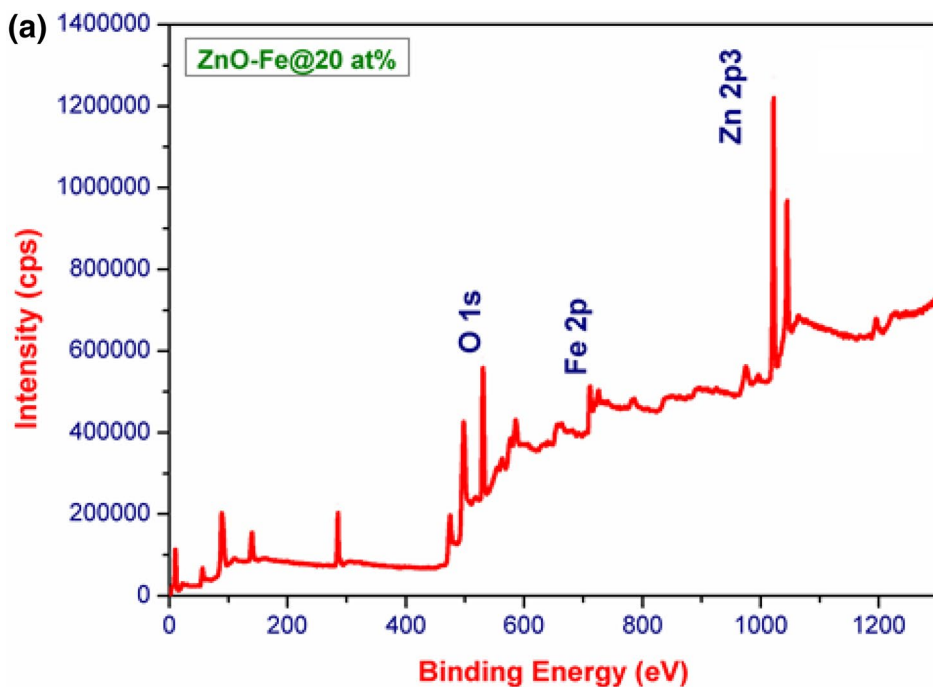
evaluation of degradation of the dye. The absorption spectra of MB dye with pure and Fe doped ZnO nanoparticles are shown in Fig. 8. From the spectra, it can be seen that the characteristic absorption of pure and Fe doped ZnO was decreased when increasing the irradiation time. It is also seen from the figure that when Fe is doped with ZnO, the characteristic peak of MB

is broadened and indicating the incorporation of Fe on ZnO. The efficiency of the prepared nanoparticles for degrading the MB dye can be calculated using the following equation [28]

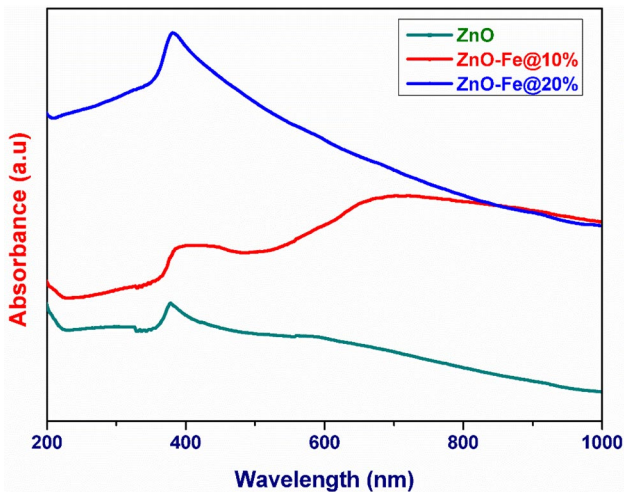$$\eta = \frac{C_0 - C_t}{C_0} \times 100 = \frac{A_0 - A_t}{A_0} \times 100 \qquad (4)$$

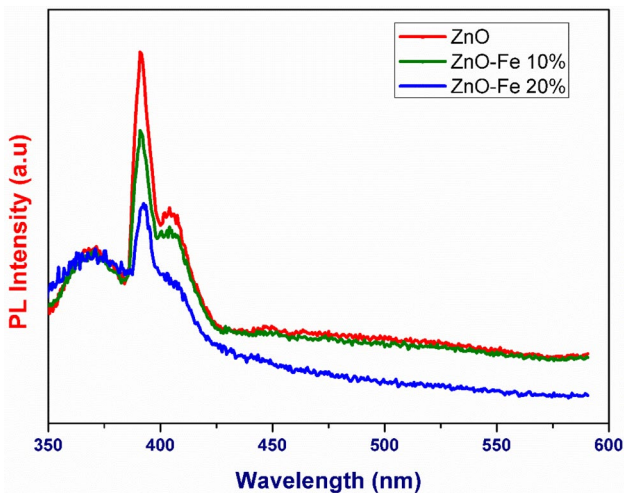**Fig. 6** UV–Vis absorbance spectra of undoped and Fe doped ZnO nanoparticles

Fig. 7 Photoluminescence spectra of undoped and Fe doped ZnO nanoparticles

where C_0, C_t, A_0, and A_t are the initial concentration, the concentration at any time t, initial absorption and absorption at any time, respectively. Table 3 shows the calculated dye degradation efficiencies of the pure and Fe doped ZnO samples. From the table values, it can be seen that the degradation efficiency increases as the doping concentration of Fe increases.

The enhancement of the photocatalytic activity may be due to the decrease in the diffusion path length of the photogenerated electrons excited by the UV visible light irradiation [29], by the reduction of crystallite size. In the case of Fe doped ZnO, the enhancement is attributed as the shifting of band edges of ZnO due to the incorporation of the Fe atoms

in the ZnO lattice. Due to the enhancement, the photon energy can easily shift the valance band electrons into the conduction band. This enhances the photocatalytic activity of the prepared Fe doped ZnO nanoparticles. This may be due to the formation of more acceptor level in the valence band. Wiem et al. [30] suggested that the incorporation of Fe in ZnO create an intermediate energy level which acts as a sink through which photogenerated electrons can easily move from the valence band to conduction band. Another important parameter that enhances the photocatalytic activity is the particle size. The particle size can be related to the photocatalytic efficiency since the reduction in particle size increases the charge transfer due to the increase of surface sites [31]. In the present study, it is evident that the particle size of Fe doped ZnO is small and enhances the charge transfer on the surface. This correspondingly increases free charge carriers and further enhances the photocatalytic efficiency. The efficiency of the prepared ZnO nanoparticles may be improved by further increase of doping or by reduction of the particle size with the use of proper surfactants.

The mechanism of the photocatalytic activity of Fe doped ZnO nanopowder is shown in the Fig. 9.

3.8 Theoretical verification of photocatalytic activity

The calculated band gaps of ZnO and Fe doped ZnO are 2.28, 2.01 and 1.91 eV, respectively. The obtained results are very low compared to experimentally observed values. This is due to the well-known reason that DFT underestimates the band gap energy because of the unknown exchange-correlation energy. However, the relative variation is well matched with the experimentally observed results. In this present study, the variation of the calculated optical bandgap is relatively comparable with the theoretically calculated values. The photocatalytic activity of pure and Fe doped ZnO can be calculated in terms of their valance and conduction bands. The oxidation capacity of holes and the reduction capacity of electrons will be correlated to the positive value of valance band maximum (VBM) and negative value of conduction band minimum (CBM), respectively [32]. The edge potentials of ZnO and Fe doped ZnO were calculated by using the electronegativity and the band gaps of the corresponding structures. They are estimated using the following relations [33].

$$E_{VB} = \chi - E_e + \frac{1}{2}E_g \tag{5}$$

$$E_{CB} = E_{VB} - E_g \tag{6}$$
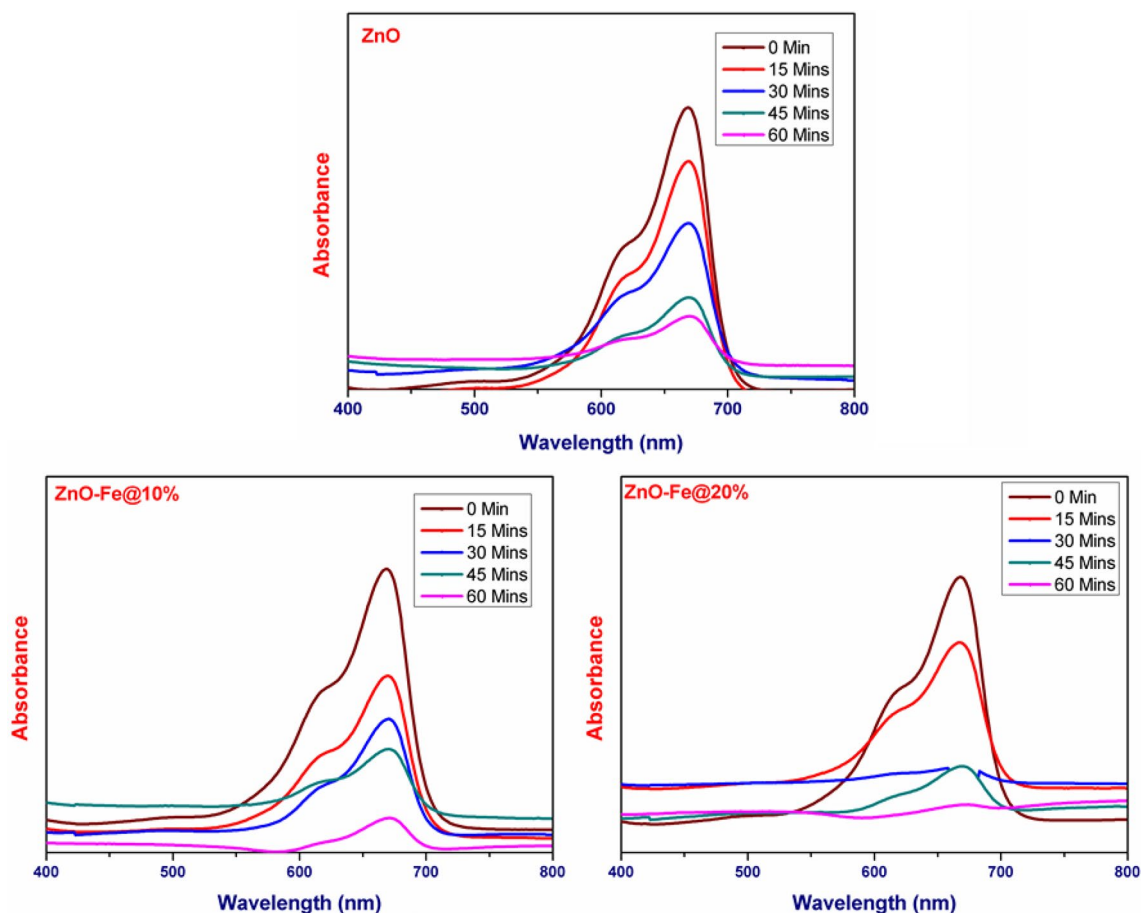
$$\chi = \frac{IP + EA}{2} \tag{7}$$

Fig. 8 Absorbance spectra of undoped and Fe doped ZnO samples

Table 3 Photocatalytic efficiency of ZnO and Fe-doped ZnO nanoparticles

S. no.	Sample	Efficiency (%)
1	ZnO	68.52
2	ZnO–Fe 10%	73.96
3	ZnO–Fe 20%	87.92

where χ is the electronegativity, E_e is the free electron energy in hydrogen scale, and E_g is the calculated band gap. The calculated band edge potentials are listed in Table 4.

In general, the degradation of organic dyes can be attributed to the oxidation of O_2^-, H_2O_2, OH and the holes. The redox potentials of O_2/H_2O_2 with respect to normal hydrogen electrode (NHE) was 1.23 V. Similarly, the photogenerated electrons will oxidize the O_2 into O_2^- since the oxidizing potential with respect to NHE was -0.33 V. From the tabulated values, it is seen that all the calculated redox potentials were found to be in the range compared to NHE and enhances the photocatalytic activity.

4 Conclusion

Undoped and Fe doped ZnO nanoparticles were prepared by a facile and cost-effective method. The XRD patterns confirm that the prepared particles have hexagonal wurtzite structure with an average crystallite size of 28 nm. A secondary peak in XRD at 27° indicates the incorporation of Fe on ZnO lattice. The TEM image reveals that the particles are spherical in nature. The crystallite size does not show any appreciable variation due to Fe doping. The XPS study confirms the presence of Fe in the ZnO lattice. The calculated optical bandgap shows shifts to lower energy region due to doping. The photocatalytic efficiency of the nanoparticles was tested against the degradation of MB dye and was found that the degradation efficiency is increased due to increase in the Fe concentration. A theoretical verification study was performed using DFT calculations to find the band edge position of pure and Fe doped ZnO nanostructures, and the results also confirm the experimental observations.

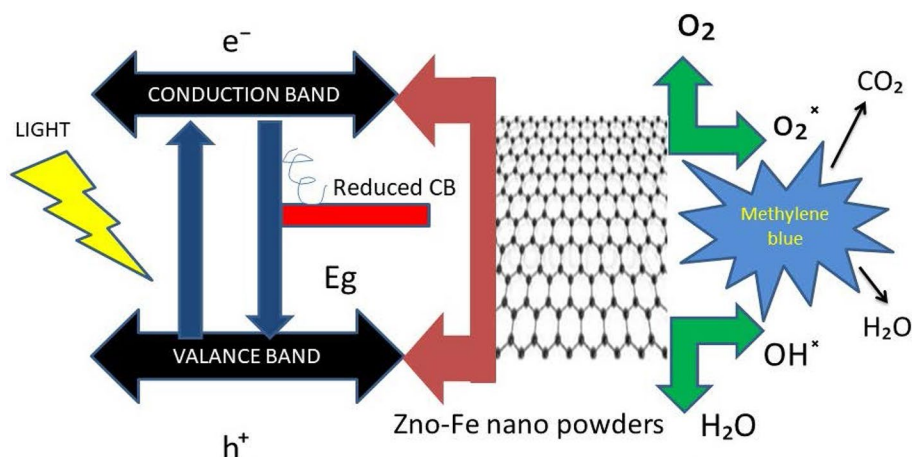**Fig. 9** Photocatalytic mechanism of Fe doped ZnO nanoparticles

Table 4 Calculated band edge potentials of ZnO and Fe-doped ZnO nanoparticles

Structure	E_{VB} (V)	E_{CB} (V)
ZnO	1.7165	− 0.5413
ZnO–Fe 10%	1.85215	− 0.43115
ZnO–Fe 20%	1.7425	− 0.5725

References

1. R.J. Tayade, P.K. Surolia, R.G. Kulkarni, R.V. Jasra, Sci. Technol. Adv. Mater. **8**, 455 (2007)
2. V. Srikant, D.R. Clarke, J. Appl. Phys. **83**, 5447 (1998)
3. E. Mollwo, in *Semiconductors: Physics of II-VI and I-VII Compounds, Semimagnetic Semiconductors*, vol. 3 of Landolt-Börnstein New Series, ed. by O. Madelung, M. Schulz, H. Weiss (Springer, Berlin, 1982), p. 35
4. Y. Hou, Z. Xu, S. Sun, Angew. Chem. Int. Ed. **46**, 6329 (2007)
5. X. Yu, D. Meng, C. Liu, K. Xu, J. Chen, C. Lu, Y. Wang, J. Mater. Sci. Mater. Electron. **25**, 3920 (2014)
6. K. Singh, V. Devi, R. Dhar, D. Mohan, Superlattices Microstruct. **85**, 433 (2015)
7. T. Srinivasulu, K. Saritha, K.T.R. Reddy, Mod. Electron. Mater. (2017). https://doi.org/10.1016/j.moem.2017.07.001
8. B.P. Kafle, S. Acharya, S. Thapa, S. Poudel, Ceram. Int. **42**, 1133 (2016)
9. A. Kumar, P. Dhiman, M. Singh, Ceram. Int. **42**, 7918 (2016)
10. R. Saleh, N.F. Djaja, Superlattices Microstruct. **74**, 217 (2014)
11. L.M.C. Pereira, U. Wah, J.G. Correia, M.J. Van Bael, K. Temst, A. Vantomme, J.P. Araujo, J. Phys. Condens. Matter **25**, 416001 (2013)
12. S.S. Kumar, P. Venkateswarlu, V. Ranga Rao, G. Nageswara Rao, Int. Nano Lett. **3**, 1 (2013)
13. S.K. Mishra, R.K. Srivastava, S.G. Prakash, J. Mater. Sci. Mater. Electron. **24**, 125 (2013)
14. J. Liu, L. Wang, S. Zhog, Y. Han, Mater. Manuf. Process. **28**, 10 (2012)
15. S.N. Bai, S.C. Wu, J. Mater. Sci. Mater. Electron **22**, 339 (2011)
16. M. Jay Chithra, K. Pushpanathan, M. Loganathan, Mater. Manuf. Process. **29**, 771 (2014)
17. K. Saravanakumar, B. Sakthivel, K. Ravichandran, Mater. Lett. **65**, 2278 (2011)
18. J.M. Soler, E. Artacho, J.D. Gale, A. Garcia, J. Junquera, P. Ordejon, D. Sanchez-Portal, J. Phys. Condens. Matter **14**, 2745 (2002)
19. J.P. Perdew, K. Burke, M. Ernzerhof, Phys. Rev. Lett. **77**, 3865 (1996)
20. K.C. Lalithambika, A. Thayumanavan, K. Ravichandran, S. Sriram, J. Mater. Sci. Mater. Electron. **28**, 2062 (2017)
21. B. Astinchap, R. Moradian, M. Nasseri, Tekyeh, Optik (Stuttg). **127**, 9871 (2016)
22. K. Saravanakumar, K. Ravichandran, R. Chandramohan, S. Gobalakrishnan, M. Chavali, Superlattices Microstruct. **52**, 528 (2012)
23. S. Kanchana, M.J. Chithra, S. Ernest, K. Pushpanathan, J. Lumin. **176**, 6 (2016)
24. A.K. Mishra, D. Das, Mater. Sci. Eng. B Solid-State Mater. Adv. Technol. **171**, 5 (2010)
25. A. Hui, J. Ma, J. Liu, Y. Bao, J. Zhang, J. Alloy. Compd. **696**, 639 (2017)
26. S. Talam, S.R. Karumuri, N. Gunnam, ISRN Nanotechnol. **22**, 2012 (2012)
27. K. Karthika, K. Ravichandran, J. Mater. Sci. Technol. **31**, 1111 (2015)
28. R. Uma, K. Ravichandran, S. Sriram, B. Sakthivel, Mater. Chem. Phys. **201**, 147 (2017)
29. L. Gomathi Devi, B. Narasimha Murthy, S.G. Kumar, Mater. Sci. Eng. B **166**, 1 (2010)
30. W. Bousslama, H. Elhouichet, M. Férid, Opt. Int. J. Light Electron Opt. **134**, 88 (2017)
31. Z. Zhang, C.C. Wang, R. Zakaria, J.Y. Ying, J. Phys. Chem. B. **102**, 10871 (1998)
32. X. Chen, S. Shen, L. Guo, S.S. Mao, Chem. Rev. (Washington, DC, United States) **110**, 6503 (2010)
33. S. Sriram. K.C. Lalithambika, A. Thayumanavan, Opt. Int. J. Light Electron. Opt. **139**, 299 (2017)